Available online at www.eccomasproceedia.org
Eccomas Proceedia COMPDYN (2025) 825- 841

ECCOMAS
Proceedia

COMPDYN 2025
10th ECCOMAS Thematic Conference on
Computational Methods in Structural Dynamics and Earthquake Engineering
M. Papadrakakis, M. Fragiadakis (eds.)
Rhodes Island, Greece, 15-18 June 2025

# EVALUATION OF EXISTING CORROSION MODELS FOR THE FLEXURAL BEHAVIOUR ASSESSMENT OF STEEL ELEMENTS SUBJECTED TO CYCLIC LOADING

**Amir Houshang Farivar Rad**[1], **José Miguel Castro**[2]

[1] PhD Student
CONSTRUCT, Faculdade de Engenharia da Universidade do Porto, Portugal
up202212318@up.pt

[2] Associated Professor
CONSTRUCT, Faculdade de Engenharia da Universidade do Porto, Portugal
Miguel.castro@fe.up.pt

## Abstract

*Corrosion significantly impacts the mechanical properties of steel and the thickness of corroded parts of steel sections, affecting existing structures' performance, especially under seismic loading. Various models have been proposed to predict the evolution of steel properties under corrosion. This study investigates the sensitivity of the flexural cyclic behaviour of steel elements to corrosion, considering various corrosion models. To achieve this, cantilever steel elements are modelled in ABAQUS, assuming different levels of corrosion through modification of both geometrical and material properties. Cyclic analyses are carried out, followed by a characterization of the cyclic behaviour that focuses on strength and deformation-related parameters. The results obtained provide valuable insights into the influence of corrosion on the ductility of steel members, as well as on the reliability of different corrosion models and their implications for structural safety evaluations.*

**Keywords:** Corrosion Effects, Flexural Cyclic Behaviour, Steel Beam, Rotation Capacity.


Peer-review under responsibility of the organizing committee of COMPDYN 2025.
doi: 10.7712/120125.12694.24614

## 1 INTRODUCTION

Corrosion is a natural and significant cause of deterioration of steel structures, affecting lifetime operation. In severe cases like strong earthquakes, it can lead to catastrophic failures, such as structural collapse, due to a reduction in load-bearing capacity. Corrosion damage can also pose life-threatening risks, making it essential to address for safety, environmental, and economic reasons. On the other hand, the structural response to seismic activity is crucial and cannot be overlooked. To accurately assess the seismic response of a structure while accounting for corrosion effects, it is essential first to analyse these effects at the structural element level. This involves examining how corrosion alters the steel member's geometry and material properties. Several experimental studies have investigated the impact of corrosion on structural steel materials [1-3]. However, accurately replicating the actual corrosion distribution in simulations is highly complex and expensive in terms of time and resources. To address this challenge, researchers have introduced the "nominal mechanical property method" [4], which correlates geometric loss due to corrosion with material property degradation. This approach enables finite element analysis of the seismic performance of corroded structures by adjusting material properties such as Young modulus and yield strength during pre-processing. Due to its practicality and ease of implementation, this method has become the standard approach for evaluating the seismic performance of corroded structures. Numerous studies have been conducted on the material properties of corroded structural steel, examining the correlation between corrosion indicators (e.g., mass loss, volume loss, and thickness reduction) and mechanical performance parameters (e.g., [5, 6]). Researchers have also developed regression models to quantify these relationships, as illustrated in Table 1. The authors cited in Table 1 primarily establish correlations between the mechanical properties of corroded steel and the mass loss ratio, which is widely recognized as a reliable indicator of corrosion effects. The mass loss ratio is typically calculated as follows:

$$D_W = \frac{m_O - m_C}{m_O} \tag{1}$$

Where $D_W$ is the specimen's mass loss ratio (the average corrosion rate), $m_O$ is the initial mass of the specimen, and $m_C$ is the residual mass of the specimen after conducting the corrosion test.

*Table 1: Regression models reflect the relationship between corrosion and the monotonic mechanical properties of steel*

| Reference Model | Yield Strength ($f_Y$) | Elastic Modulus ($E_S$) | Tensile Strength ($f_U$) | Elongation (δ) | Necking Strain ($\varepsilon_U$) | Failure Strain ($\varepsilon_f$) |
|---|---|---|---|---|---|---|
| Shi et al. [7] | * | | * | * | | |
| Garbatov et al. [8] | * | * | * | * | | |
| Zheng et al. [9] | * | * | * | * | | |
| Shanhua et al. [10] | * | | * | * | | |
| Sehng & Xia [11] | * | | * | | | |
| Li et al. [12] | * | | * | | | * |
| Wang et al. [13] | * | | * | * | | |
| Bin et al. [14] | * | * | * | * | | |
| Shanhua et al. [15] | * | * | * | | | * |
| Jia et al. [16] | * | | * | | * | * |
| Woloszyk et Garbatov [17] | * | * | * | * | | |
| Zhang et al. [18] | * | * | * | * | | |
| Wang et al. [19] | * | * | * | | * | |
| Chen et al. [20] | * | * | * | | * | |
| Si et al. [21] | * | * | * | | | * |

| | | | | | | |
|---|---|---|---|---|---|---|
| Jin et al. [22] | * | | * | * | | |
| Kong et al. [23] | * | * | * | * | | * |
| Zhang et al. [24] | * | * | * | * | | |
| Zhang et al. [25] | * | * | * | * | | |
| Wang et al. [26] | * | * | * | | * | |
| Chen et al. [27] | * | * | * | * | | |
| Kong et al. [28] | * | * | * | * | | |
| Xiao et al. [29] | * | | * | * | | |
| Xiao et al. [30] | * | | * | * | | |

As presented in Table 1, several researchers have proposed predictive models for the monotonic properties of corroded steel materials. It should be noted that the models listed in Table 1 are primarily based on mild steel (with only one case involving high-strength steel), and the corrosion tests conducted to develop them were mainly based on neutral salt spray, chloride or hydrochloric acid/salt environments, and copper accelerated acetate spray (CASS) tests. The effect of pitting corrosion is also considered in the models referenced in [11, 17, 22, and 27].

This study aims to evaluate the sensitivity of a steel member's flexural cyclic behaviour to the various models available for predicting the impact of corrosion on structural steel. Accounting for the cyclic parameters of steel in finite element modelling is essential to analyse the cyclic behaviour of steel elements. The critical parameters for steel material modelling, considering both isotropic and kinematic hardening, are listed in Table 2. As shown in the table, all of these parameters, except density, are affected by corrosive agents.

*Table 2: Effective parameters for the steel material modelling in FE analyses considering combined hardening*

| **Steel Material Parameter** | **Does it need a model (Y/N)** | **Is there any model? (Y/N)** |
|---|---|---|
| Mass density | N | N |
| Young modulus ($\mathbf{E_s}$) | Y | Y |
| Poisson's ratio ($\boldsymbol{\nu}$) | Y | Y |
| Yield strength at plastic strain equal to zero ($\boldsymbol{\sigma_0}$) | Y | Y |
| Kinematic hardening modulus ($\mathbf{C_i}$) | Y | **N** |
| The saturation parameter ($\boldsymbol{\gamma_i}$), which is associated with the nonlinear kinematic hardening component (governs the rate at which kinematic hardening reaches saturation). | Y | **N** |
| Equivalent/current yield strength ($\boldsymbol{\sigma_{eq,y}}$) | Y | Y |
| The asymptotic hardening value ($\mathbf{Q_\infty}$) represents the maximum increase in yield stress the material can reach after extensive plastic deformation (isotropic hardening). | Y | **N** |
| Hardening parameter **b** is the rate at which the material approaches $Q_\infty$ with increasing plastic strain. | Y | **N** |

As shown in Table 1, while some mechanical properties of structural steel have established models, key parameters related to cyclic behaviour—such as kinematic hardening modulus, saturation parameter, asymptotic hardening value, and hardening parameter—lack suitable models for incorporating corrosion effects. Consequently, assumptions must be made to account for these effects in FE simulations. This fact and the ones mentioned earlier highlight the need to develop more reliable models when accounting for corrosion effects on the seismic assessment of structures. In other words, there is an obvious need for more experimental studies on the corrosion effects on steel plates/members' monotonic and cyclic behaviour with a broader range of corrosion rates. However, kinematic hardening influences yield stress by altering the material's response to applied stress by translating the yield surface [31, 32]. In contrast, isotropic hardening affects the material's overall strength, including tensile strength, by expanding the yield surface and increasing resistance to plastic deformation [31-33]. Therefore, in this work, kinematic and isotropic hardening are assumed to undergo proportional changes due to corrosion, similar to yield and tensile strength. Consequently, Equations (2) and (3) apply corrosion effects to isotropic and kinematic hardening, respectively.

$$Q_{\infty}^{corroded} = Q_{\infty}^{uncorroded} \times \left(\frac{\sigma_u^{corroded}}{\sigma_u^{uncorroded}}\right) \tag{2}$$

$$C_i^{corroded} = C_i^{uncorroded} \times \left(\frac{\sigma_y^{corroded}}{\sigma_y^{uncorroded}}\right) \tag{3}$$

Since the saturation parameter ($\gamma_i$) and hardening parameter ($b$) are rate parameters, it is assumed that the corrosion will not affect them.

In this study, a nonlinear model of a steel cantilever beam subjected to cyclic loading has been investigated, considering various predictive models of corrosion effects on steel, the assumptions made regarding the cyclic parameters of the steel material, and three different corrosion damage rates. Details of the studied model will be presented in the corresponding section. Subsequently, the results of the cyclic analyses are presented and compared, focusing on flexural strength and deformation capacity. Finally, the implications of the findings for structural safety assessments and future research directions are discussed.

## 2 COMPARISON OF EXISTING PREDICTIVE MODELS FOR CORROSION EFFECTS ON STRUCTURAL STEEL PROPERTIES

As shown in Table 1, various models have been proposed to date for evaluating the effects of corrosion on the monotonic mechanical properties of structural steel. Figure 1 illustrates the evolution of the monotonic mechanical properties of steel material as a function of the corrosion rate, expressed in terms of mass loss. As shown, material properties such as yield strength, tensile strength, elongation, and Young modulus decrease as the corrosion rate increases. However, discrepancies between different models are evident. Additionally, many models have been derived based on mass loss ratios lower than 20%, whereas in the current study, a mass loss ratio of 30% is also considered.

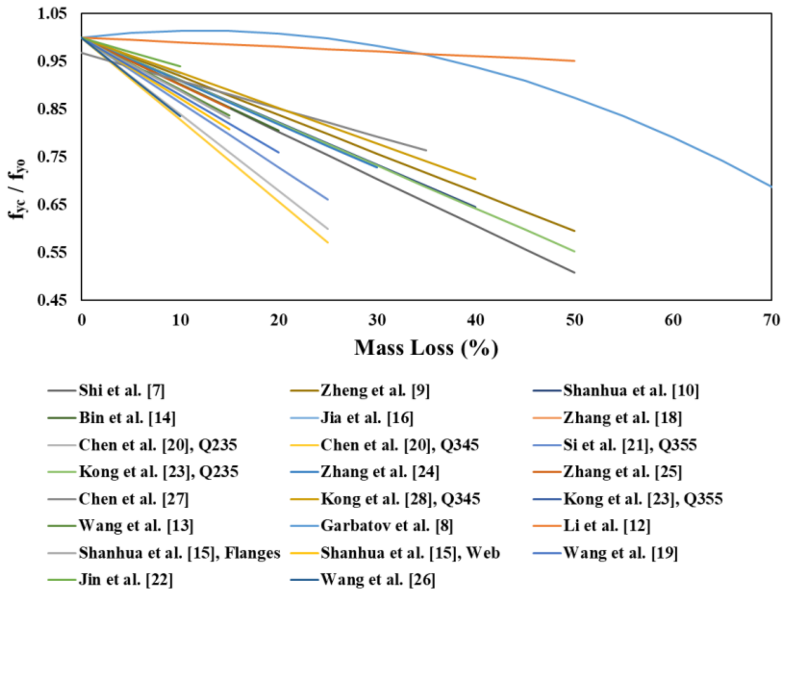


*(a)*

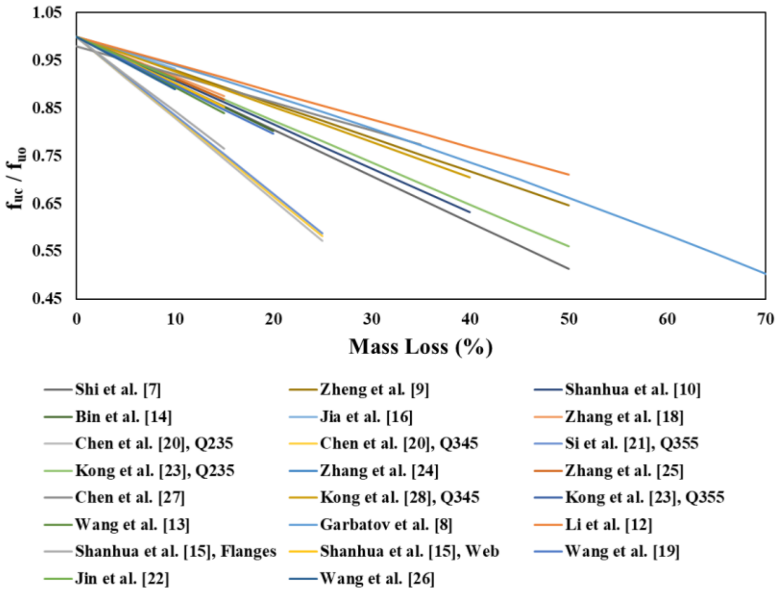


*(b)*

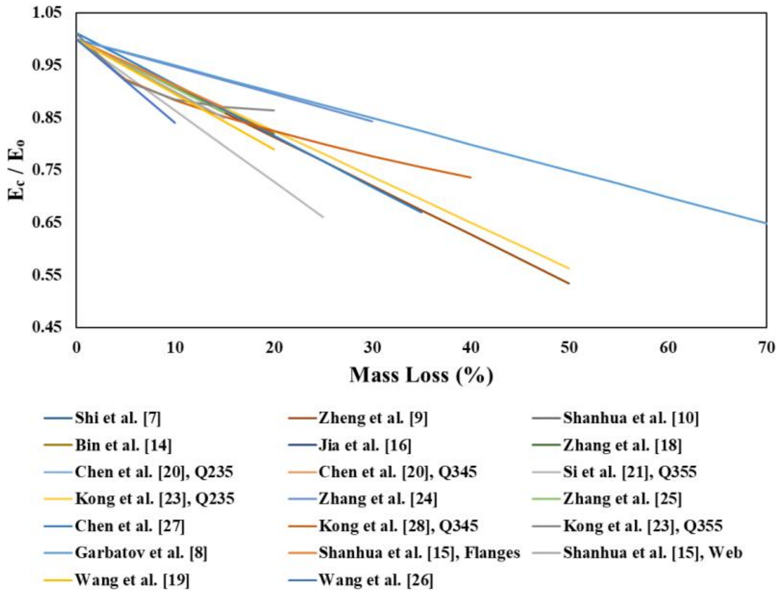


*(c)*

*Figure 1: Evolution of monotonic mechanical properties of steel material considering corrosion effects. (a) yield strength, (b) tensile strength, and (c) Young modulus.*

## 3 MODEL DESCRIPTION

A 3D finite element model was developed using the commercial software ABAQUS® [34] to investigate the sensitivity of the flexural cyclic behaviour of steel elements to different predictive corrosion models. The model represents a cantilever beam, simulating the behaviour of a beam segment from one end to the point of inflection, assumed to be at the mid-length of the member. The finite element model used in this study is illustrated in Figure 2. To enforce fixed boundary conditions, one edge was fully restrained. Cyclic loading was applied to the free edge of the beam, which was restrained in the X-X direction to prevent out-of-plane displacements, following the experimental setup of D'Aniello et al. [35]. This study adopted the symmetric cyclic loading protocol outlined in ANSI/AISC 341-16 [36], illustrated in Figure 3.

Cyclic loading was applied as end displacements with an amplitude history along the beam's strong (y-y) axis, imposed at reference point RP-2. Both cross-section edges were constrained as rigid bodies to reference points RP-1 and RP-2 to prevent stress concentration. The beam's plates were modelled using quadratic shell elements (S4R), which are well-suited for capturing large inelastic deformations and post-buckling behaviour. A highly refined mesh with a 10 mm edge size was used, maintaining a consistent mesh density along the entire member length to accurately simulate potential lateral and torsional buckling (LTB). Additionally, lateral restraints were applied to the flanges to limit excessive LTB. The unbraced length ($L_b$), defined as the distance between lateral restraints, was considered based on ANSI/AISC 341-16 [36] using Eq. (4).

$$L_b = 0.095 i_z \left(\frac{E}{F_y}\right) \tag{4}$$

Where $i_z$ is the radius of gyration of the cross-section, $E$ is the Young modulus, and $F_y$ is the steel yield stress. Flange and web imperfections were incorporated into the model by considering the geometrical manufacturing tolerances specified in EN 10034 [37]. Geometrical imperfections were explicitly incorporated into the numerical model based on the shape and dimensional tolerances specified in the European Standard EN 10034 [37] for I and H beams, following the approach used by Elkady and Lignos [38]. As illustrated in Figure 4, flange imperfections were modelled using symmetric out-of-squareness deviations from the nominal section. The amplitudes assigned were 2% for flange imperfections and 0.4% for web imperfections. The 2% value represents the maximum tolerance allowed by EN 10034 [37] for sections with a flange width *b≥110 mm*, while the 0.4% value was determined based on engineering judgment and recommendations found in the literature [38]. Table 3 represents the combination of imperfection types and their respective amplitudes.

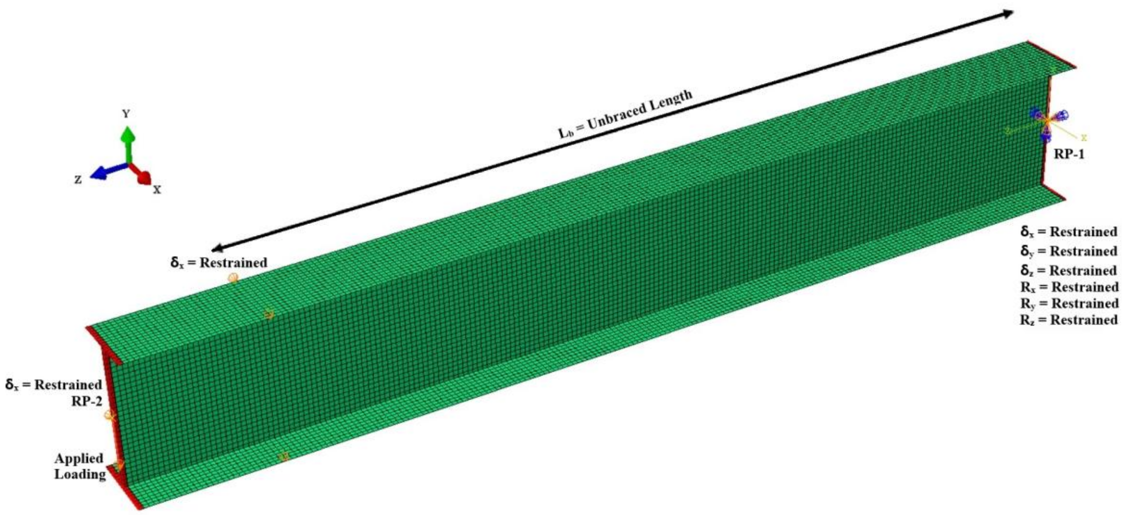


*Figure 2: Finite element model*

*Table 3: Considered imperfections in the modelling*

| Imperfection Type | K + K' | e |
|---|---|---|
| **Flange (symmetric) + Web** | 2% b | 0.4% h |

To accurately simulate the complex cyclic behaviour of the material, a combined nonlinear isotropic/kinematic hardening plasticity model, based on Chaboche's formulation [39], was implemented using the ABAQUS materials library. The mathematical representation of the nonlinear isotropic component is given in Eq. (5), which accounts for the material's cyclic hardening or softening behaviour by expanding or contracting the Mises yield surface.

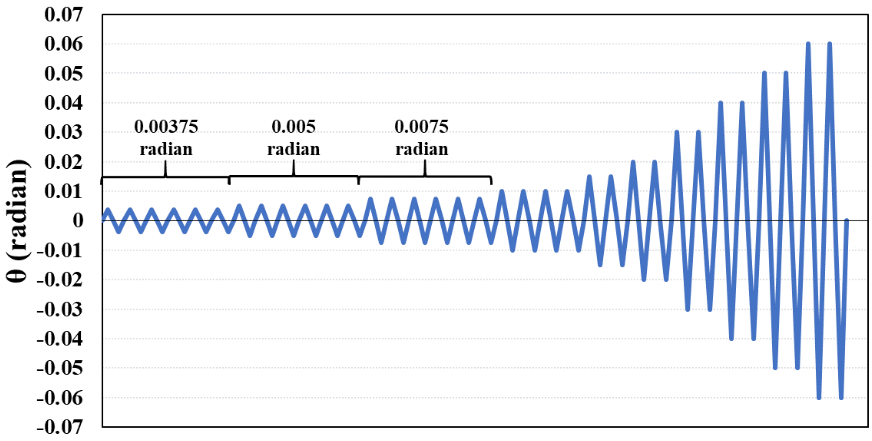


*Figure 3: Cyclic Loading Protocol (AISC41-16: K2.4b)*

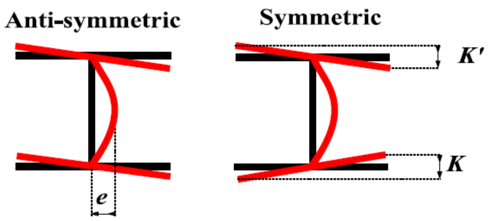


*Figure 4: Geometrical imperfections considered in the FE model*

The nonlinear kinematic hardening component models the translation of the yield surface in stress space through the backstress vector $\alpha$. This mechanism enables the representation of complex effects such as the Bauschinger effect. The evolution law for the backstress, which governs the movement of the Mises yield surface centre, is mathematically expressed in Eq. (6).

$$S^0 = S|_0 + Q_\infty \left(1 - e^{-be^{pl}}\right) \tag{5}$$

$$\dot{\alpha}_k = C_k \frac{1}{S^0}(s - \alpha)\dot{\bar{e}}^{pl} - g_k a_k \dot{\bar{e}}^{pl} \tag{6}$$

The cyclic plasticity model was calibrated using cyclic stress-strain data obtained from tests conducted under ascending and alternating loading protocols, as reported by Chen et al. [40]. The material model parameters for Chinese steel grades Q235c, Q235b, and Q345b, which are equivalent to the European steel grades S235 and S355, are calculated based on the steel material grade of the references listed in Table 1. The cantilever beam studied has an IPE300 section with a 2-meter length and an unbraced length ($L_b$) of 1.72 meters. The physical test on the IPE300 section conducted by D'Aniello et al. [35] was replicated in ABAQUS to validate the finite element model developed in this study while considering uncorroded steel material since the referenced test was conducted on an uncorroded steel beam. The hardening parameters of uncorroded steel grade Q345b were used in the simulation (E=177370 MPa, $\sigma_0$=280 MPa, $Q_\infty$=113 MPa, b=1.3, $C_1$=11578 MPa, $\gamma_1$=182, $C_2$=4350.5 MPa, and $\gamma_2$=42), because its yield strength matches that of the tested specimens. Figure 5a compares the moment-chord rotation cyclic curves obtained from the numerical model and the experimental results. As it can be observed, the numerical and experimental outcomes demonstrated good agreement.

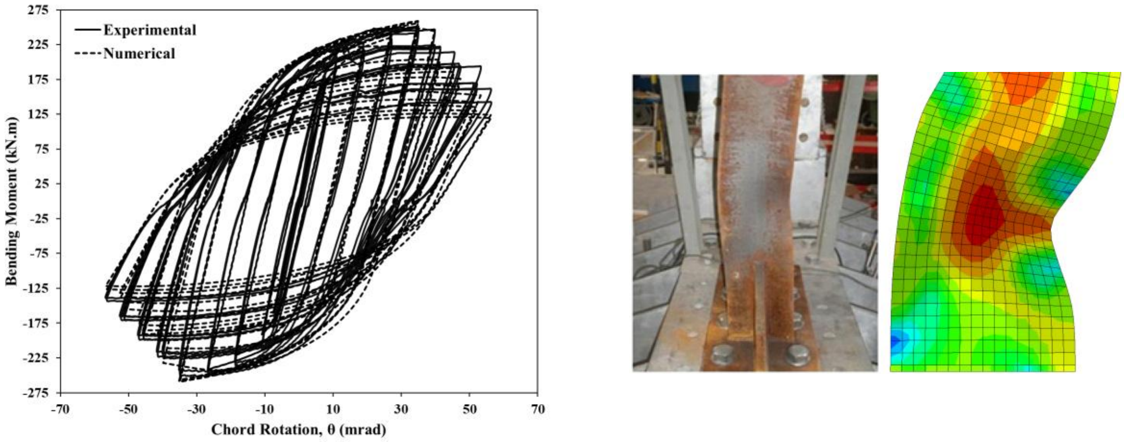


*(a)* *(b)*

*Figure 5: Comparison between experimental and numerical results. (a) Moment-Chord Rotation Curve, (b) Plastic deformation involving local buckling*

Figure 5b compares the failure modes observed in the experiments and the numerical simulation. The numerical model effectively captured the local buckling patterns, accurately replicating the lateral and torsional buckling exhibited by the IPE300 member.

*Table 4: Simulation cases considered in this study*

| Case Name | Corroded Part (in the plastic hinge region) | Corrosion Rate (%) | Section part thickness in the corroded region ** | Cyclic Hardening Tag |
|---|---|---|---|---|
| BTF | Both flanges | 10% | $t_{fc} = 0.9t_{fo}$<br>$t_w$ remains unchanged | NDC<br>DC |
| | | 20% | $t_{fc} = 0.8t_{fo}$<br>$t_w$ remains unchanged | NDC<br>DC |
| | | 30% | $t_{fc} = 0.7t_{fo}$<br>$t_w$ remains unchanged | NDC<br>DC |
| W | Only Web | 10% | $t_f$ remains unchanged<br>$t_{wc} = 0.9t_{wo}$ | NDC<br>DC |
| | | 20% | $t_f$ remains unchanged<br>$t_{wc} = 0.8t_{wo}$ | NDC<br>DC |
| | | 30% | $t_f$ remains unchanged<br>$t_{wc} = 0.7t_{wo}$ | NDC<br>DC |
| FS | Full Section | 10% | $t_{fc} = 0.9t_{fo}$<br>$t_{wc} = 0.9t_{wo}$ | NDC |
| | | 20% | $t_{fc} = 0.8t_{fo}$<br>$t_{wc} = 0.8t_{wo}$ | |
| | | 30% | $t_{fc} = 0.7t_{fo}$<br>$t_{wc} = 0.7t_{wo}$ | |

** $t_{fo}$ and $t_{fc}$ represent the original and corroded flange thicknesses, respectively, while $t_{wo}$ and $t_{wc}$ denote the original and corroded web thicknesses.

This study assumes that corrosion uniformly affects the entire plastic hinge region over a length of $1.5d_b$ from RP-1 (the fixed end of the cantilever beam), corresponding to 450 mm for the studied IPE300 section. It is considered that corrosion reduces the thickness of the flanges, web, or entire section's thickness while also modifying the material properties of the corroded region. The models presented in Table 1 and Equations 2 and 3 are adopted to update the material properties of the steel in the corroded region. Consequently, the corrosion effect on the steel beam was applied accordingly, with different thicknesses assigned to corresponding parts of the studied beam. Three different corrosion rates are applied to the models, corresponding to 10%, 20%, and 30% of mass loss in terms of thickness reduction. Additionally, as previously mentioned, kinematic and isotropic hardening are assumed to change proportionally due to corrosion, similar to yield and tensile strength. To account for this, two different conditions are considered in the numerical analysis: one where the cyclic hardening parameters are affected by corrosion (DC: Degradation of Cyclic hardening parameters) and another where these parameters remain unchanged, identical to the original steel material (NDC: No Degradation of Cyclic hardening parameters). Table 4 presents the different cases analysed in this study. According to Tables 1 and 4, 174 cyclic nonlinear analyses were conducted in ABAQUS® [34] using a continuum finite element model capable of accurately simulating steel members' buckling and post-buckling behaviour under cyclic loading.

## 4 RESULTS AND DISCUSSION

As previously stated, this study examines the impact of corrosion on the flexural cyclic behaviour of steel beams using existing predictive models in the literature for the evolution of the mechanical properties of steel material. Consequently, this section explores the influence of corrosion on variations in flexural strength and deformation parameters and the sensitivity of these parameters to different predictive models available in the literature.

Part 3 of Eurocode 8 (EC8-3) [41] defines three performance limit states: Damage Limitation (DL), Significant Damage (SD), and Near Collapse (NC). For steel beams, these damage states are quantified using the ductility ratio $\mu=\theta_P/\theta_y$, where $\theta_P$ represents the beam's plastic rotation, calculated by subtracting the chord rotation at yielding ($\theta_y$) from the total chord rotation ($\theta$). According to the code, for ductility class 1 beams, the plastic rotation limits corresponding to DL, SD, and NC are $1\theta_y$, $6\theta_y$, and $8\theta_y$, respectively.

EC8-3 [41] specifies that at the DL limit state, only minimal plastic deformations are allowed; at the SD limit state, beams should develop their full plastic moment without experiencing geometric instabilities; and at the NC limit state, the member undergoes geometric instabilities such as local buckling. However, local buckling can develop under cyclic loading at relatively low plastic deformation levels, significantly reducing the interval between DL and SD. In contrast, ASCE41-06 [42] allows local buckling of beam elements and severe joint distortion at the same plastic rotation levels corresponding to the SD limit state of EC8-3. Several experimental studies have shown that flange buckling can occur at an early stage without causing a reduction in bending strength (e.g., Zieman [43]). Identifying the onset of local buckling from moment-rotation hysteresis curves becomes challenging in such cases. This may lead to uncertainty in determining the Damage Limitation (DL) and Significant Damage (SD) limits. As a result, defining the rotation at DL is beyond the scope of this study.

Following commonly adopted definitions in the literature [44, 45], the rotation capacity limit at SD is taken as the plastic rotation at the maximum moment ($\theta_{Pmax}$) obtained from the hysteresis curve. Meanwhile, in this work, the rotation at Near Collapse ($\theta_{P80\%}$) is defined hereafter as the rotation at which the bending strength decreases to 80% of the maximum moment in the descending slope of the first-cycle envelope. Figure 6 illustrates the performance limits considered in this study, along with the cyclic moment-rotation curve and the backbone curve.

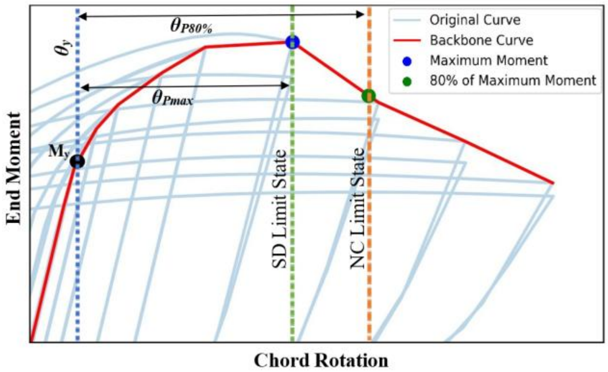


*Figure 6: Definition of damage states based on plastic rotation thresholds*

Beyond the NC limit, cyclic degradation continues until the member fully collapses. Although the rotation at collapse is relevant for collapse analysis, the beam undergoes significant plastic deformations at this stage, which can lead to ultra-low cycle fatigue or cracks in connection components—phenomena not accounted for in this study's numerical model. Therefore, accurately estimating the rotation at collapse falls outside the scope of this research. A conservative approach could be to extrapolate $\theta_{P80\%}$ to zero bending moment, though this does not account for residual stabilized hysteresis at large deformations.

The plastic rotations $\theta_{Pmax}$ and $\theta_{P80\%}$ are calculated using Equations (7) and (8), where $\theta_y$ represents the rotation at yielding ($\theta_y = \frac{M_y L}{3EI}$), $M_y$ is the bending moment at yielding, $L$ is the cantilever beam length, $E$ is the Young modulus of steel, and $I$ is the moment of inertia.

$$\theta_{Pmax} = \theta_{max} - \theta_y \tag{7}$$

$$\theta_{P80\%} = \theta_{80\%} - \theta_y \tag{8}$$

Figure 7 illustrates the flexural cyclic behaviour of the analysed steel cantilever beam for Q235C steel grade while considering the corresponding predictive models for corrosion effects on steel Q235C material, as outlined in Table 1 and the cases listed in Table 4. Additionally, these results highlight the point corresponding to the attainment of the NC limit state. As illustrated in Figure 7, corrosion considerably decreases the flexural strength of the beam and the corresponding rotation capacity within the corroded region, specifically the plastic hinge zone. However, a comparison between Figures 7a and 7b reveals that, as anticipated, the flexural strength and rotation capacity reduction is more pronounced when corrosion affects the flanges than when it is limited to the web. Additionally, Figure 7 highlights how different models for incorporating corrosion effects influence the section's flexural strength and rotation capacity. Since applying different models can yield varying flexural strengths and rotation capacities for the same steel profile, it follows that the strength of a corroded beam is highly dependent on the chosen corrosion model. Therefore, the variability and discrepancies among the available models in the literature should be carefully accounted for when assessing the flexural cyclic behaviour of corroded steel members. For example, when applying a 30% corrosion rate to both flanges of the studied IPE300 beam, the minimum reduction in the $0.8M_{max}$ value—representing the flexural strength at the NC limit state—is 68.5% based on the corrosion models outlined in [10]. In contrast, the maximum reduction reaches 72.1% when using the corrosion models presented in [9], compared to the uncorroded cantilever steel beam.

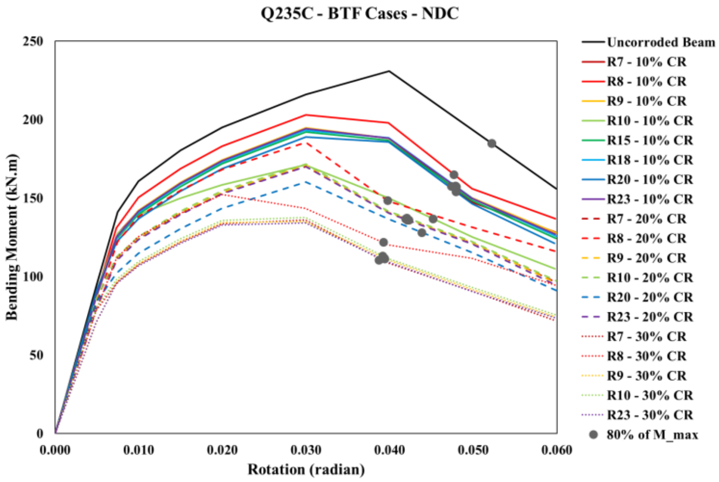


*(a)*

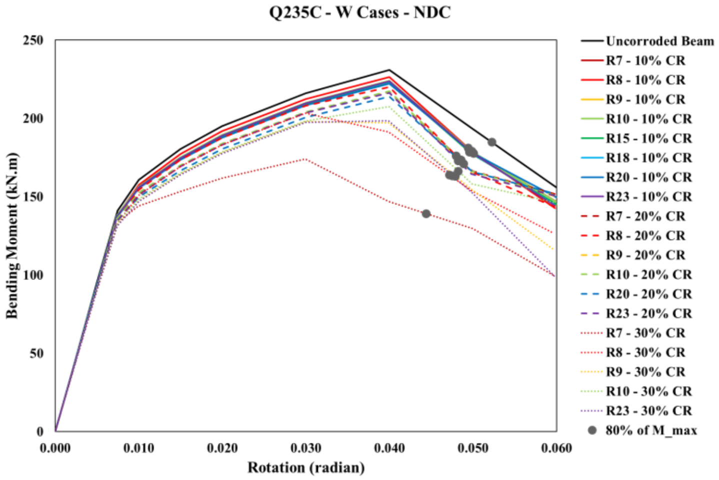


*(b)*

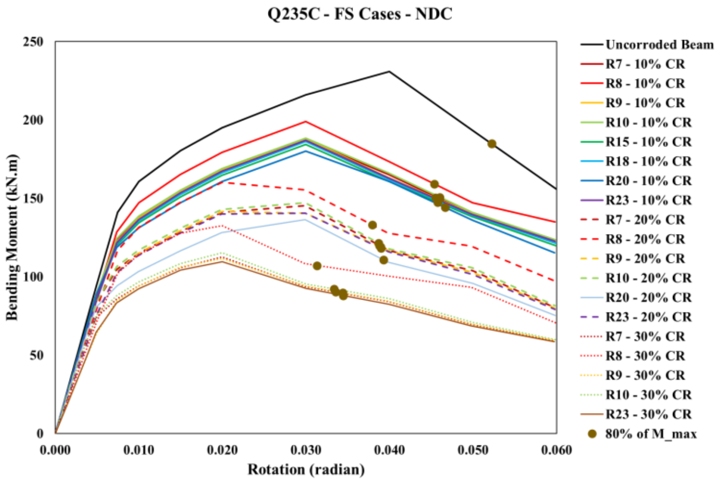


*(c)*

*Figure 7: Backbone curves of the plastic hinge flexural cyclic response of the IPE300 beam, considering the corrosion models outlined in Table 1 for Q235C steel material, and with the NDC condition for cyclic hardening parameters: (a) BTF cases, (b) W cases, and (c) FS cases, as described in Table 4.*

Figure 8 summarises the moment-rotation behaviour of the studied IPE300 cantilever beam at the NC limit state for all predictive corrosion models listed in Table 1, regardless of the steel grades used in this study. Figure 8 shows that, as the corrosion rate of the steel section increases—particularly in the flanges of the studied IPE300, the reduction in the rotational capacity of the profile also becomes more significant. Although part of the dispersion in the moment-rotation behaviour of the profile is due to the difference in steel grade used based on the models listed in Table 1, as shown in Figure 7 (for one specific steel grade), the model applied to account for the corrosion effect on the structural steel significantly influences the dispersion of the behaviour for the same profile. This effect should be properly considered in corroded steel members' seismic and cyclic analysis.

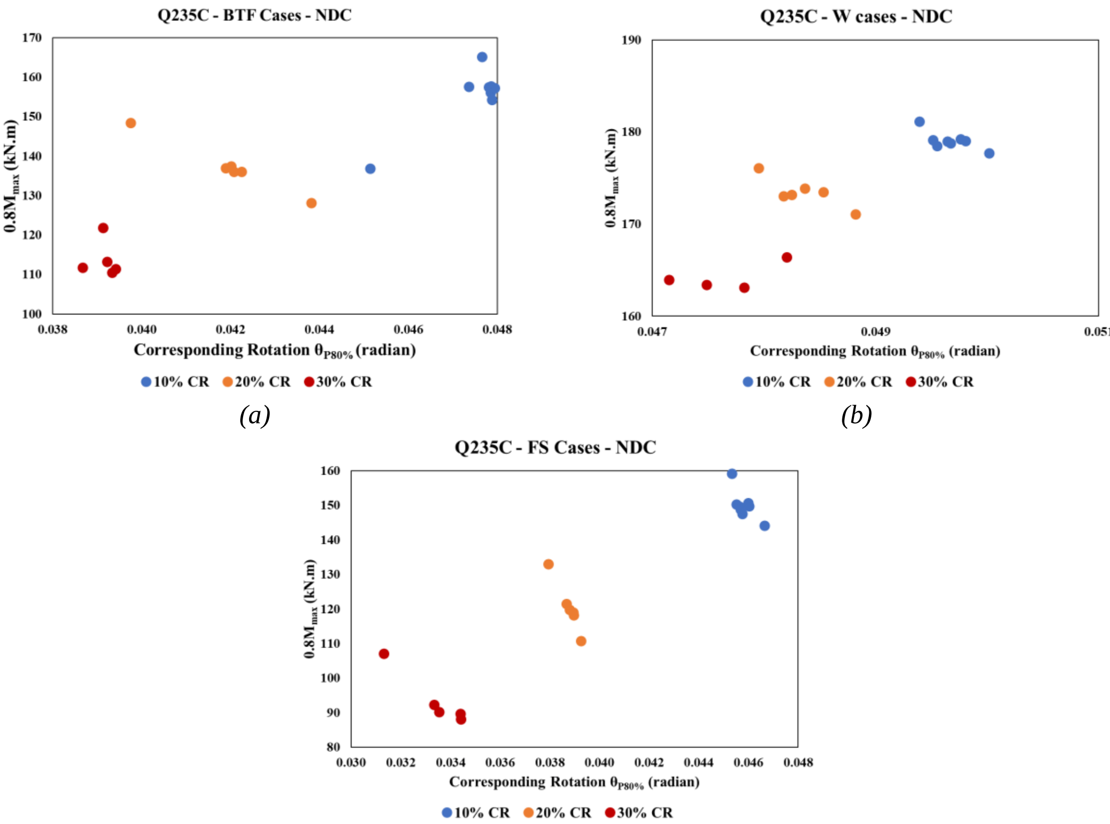


(c)

*Figure 8: Moment-rotation behaviour of the IPE300 beam at the NC limit state, considering the corrosion models outlined in Table 1 for Q235C steel material, and with the NDC condition for cyclic hardening parameters: (a) BTF cases, (b) W cases, and (c) FS cases, as described in Table 4.*

In the cyclic analysis of steel beams, dissipated energy is a key parameter in assessing structural performance under repeated loading. It reflects the energy absorbed and dissipated through plastic deformations, material hardening, and local instabilities such as buckling [31]. The area enclosed by the hysteresis loops in a moment-rotation curve quantifies the dissipated energy, with larger loops indicating greater energy dissipation capacity [46]. This ability to dissipate energy is critical for evaluating a beam’s resistance to seismic loading, as it directly influences structural ductility and stability [47]. However, corrosion and material degradation can significantly reduce the energy dissipation capacity of the steel member by weakening the beam’s strength and stiffness, potentially leading to premature failure. It also increases plate slenderness, increasing the potential for earlier local buckling. Therefore, assessing the dissipated energy under cyclic loading is essential for understanding a beam’s durability and predicting its long-term performance [48]. Figure 9 shows both the total dissipated energy and the energy dissipated by the plastic hinge of the studied model up to the NC limit state, considering the models presented in [7] that predict the effect of corrosion on structural steel and accounting for the BTF cases outlined in Table 4. As shown in Figure 9, for each level of corrosion, the difference between the two NDC and DC conditions is less than 3%. Therefore, although it is important to explore the effects of corrosion on the cyclic hardening parameters of steel material, the results for the NDC condition are reported in almost all graphs in this study.

Figure 10 shows the total energy dissipated by the plastic hinge of the studied numerical model, considering the predictive models to account for corrosion effects on the Q235C steel presented in Table 1 and the NDC condition described in Table 4. The dispersion of results for each corrosion level highlights the sensitivity of the structural behaviour to the predictive models available in the literature. Therefore, as observed for other engineering demand parameters of the studied steel beam—such as rotation capacity and flexural strength, using different models to apply corrosion effects to structural steel can lead to variable results.

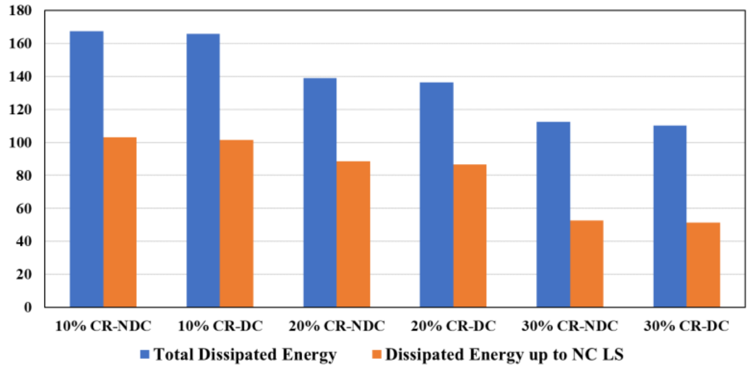


*Figure 9: Comparison of the energy dissipated by the studied model under NDC and DC conditions*

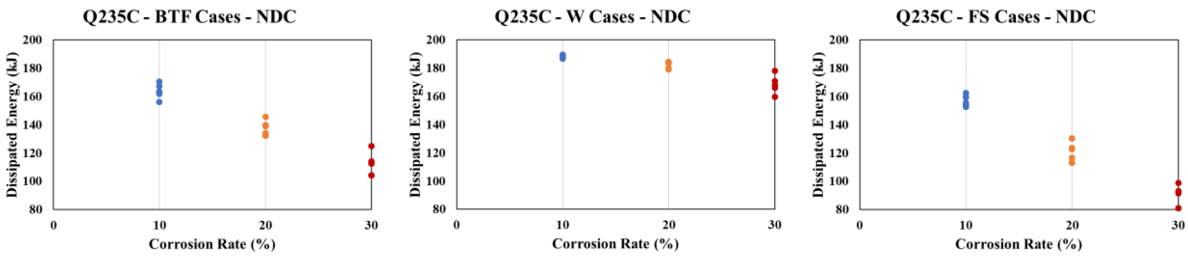


*Figure 10: Comparison of the total dissipated energy of the studied model considering the corrosion models outlined in Table 1 for Q235C steel material and with the NDC condition for cyclic hardening parameters: (a) BTF cases, (b) W cases, and (C) FS cases outlined in Table 4*

## 5 CONCLUSIONS

Based on the findings of this study, the following conclusions are drawn.

Effect of Corrosion on Flexural Cyclic Behaviour: This study confirms that corrosion significantly impacts the flexural cyclic behaviour of steel elements, mainly by reducing bending strength and stiffness as well as rotation and energy dissipation capacities. The results indicate that the effect is more pronounced when corrosion affects the flanges than the web of an I-shaped steel section. Furthermore, considering the corrosion effects on the steel material in structural and seismic analyses is essential. Even low levels of corrosion can significantly influence the seismic behaviour of steel members and structures, potentially leading to unexpected failure modes compared to those predicted at the time of design based on the properties of the uncorroded section. Besides, the deterioration of cyclic hardening parameters has a minor influence on dissipated energy, suggesting that existing corrosion models may require further refinement to capture these effects accurately.

Variation in Corrosion Models and Structural Behaviour: The findings reveal significant variation among predictive models for corrosion effects on structural steel. Different models yield notably different values for flexural strength and rotation capacity, indicating that the choice of predictive model can substantially impact seismic or cyclic assessments of corroded structures. This underscores the need for improved, experimentally validated models for a broader range of corrosion conditions.

Recommendations for Future Research and Structural Safety: Given the observed differences among existing models and the limited experimental data on the cyclic properties of corroded steel, further research is needed. Experimental validation of corrosion effects at higher mass loss ratios is essential for developing more reliable predictive models. Additionally, incorporating corrosion effects into seismic safety assessments could enhance structural reliability evaluations, particularly for ageing infrastructure in earthquake-prone regions.

## 6 ACKNOWLEDGMENT

The first author acknowledges the financial support provided by FCT (Fundação para a Ciência e a Tecnologia) through the PhD grant with reference 2023.03782.BD. This work results from Agenda "R2UTechnologies - Modular Systems", contract C644876810-00000019, investment project 48, funded by the Recovery and Resilience Plan (PRR) and the European Union – Next Generation EU.

This work was financially supported by Base Funding - UIDB/04708/2020 with DOI 10.54499/UIDB/04708/2020 (https://doi.org/10.54499/UIDB/04708/2020) of the CONSTRUCT - Instituto de I&D em Estruturas e Construções - funded by national funds through the FCT/MCTES (PIDDAC).

## REFERENCES

[1] S. Xu, H. Zhang, and Y. Wang, "Estimation of the properties of corroded steel plates exposed to salt-spray atmosphere," *Corrosion Engineering Science and Technology*, vol. 54, no. 5, 2019, doi: 10.1080/1478422X.2019.1613779.

[2] Z. Chen, S. Nie, W. Han, M. Tang, B. Yang, and M. Elchalakani, "A study on static properties of high-performance steel after corrosion damage," *J Constr Steel Res*, vol. 207, 2023, doi: 10.1016/j.jcsr.2023.107970.

[3] Y. Chen, B. Ma, and R. Lu, "Experimental Assessment of Mechanical Properties of Corroded Low–Alloy Structural Steel," *Buildings*, vol. 14, no. 5, 2024, doi: 10.3390/buildings14051457.

[4] Y. Wang, S. Xu, H. Wang, and A. Li, "Predicting the residual strength and deformability of corroded steel plate based on the corrosion morphology," *Constr Build Mater*, vol. 152, pp. 777–793, 2017, doi: https://doi.org/10.1016/j.conbuildmat.2017.07.035.

[5] M. Reza Khedmati, M. Mahdi Roshanali, and Z. H. Mohammad Esmaeil Nouri, "Strength of steel plates with both-sides randomly distributed with corrosion wastage under uniaxial compression," *Thin-Walled Structures*, vol. 49, no. 2, 2011, doi: 10.1016/j.tws.2010.10.002.

[6] M. R. Khedmati, Z. H. M. E. Nouri, and K. Moradidohezari, "A computational investigation of the effects of both-sides general corrosion on the buckling/plastic collapse

behaviour and strength of stiffened plates," *J Mar Sci Technol*, vol. 17, no. 1, 2012, doi: 10.1007/s00773-011-0146-x.

[7] Y. Z. Shi, L. W. Tong, Y. Y. Chen, Z. G. Li, and Kai Shen, "Experimental study on the effect of corrosion on the mechanical properties of steel and steel beams," *Journal of Building Structures*, vol. 33, no. 7, pp. 53–60, 2012.

[8] Y. Garbatov, C. Guedes Soares, J. Parunov, and J. Kodvanj, "Tensile strength assessment of corroded small scale specimens," *Corros Sci*, vol. 85, 2014, doi: 10.1016/j.corsci.2014.04.031.

[9] S. Zheng, X. Wang, L. Sun, J. Tian, Y. Han, and X. Zhang, "Experimental research on seismic behavior of multi-aged steel frame joint under acidic atmospheric environment," *Jianzhu Jiegou Xuebao/Journal of Building Structures*, vol. 36, no. 10, 2015, doi: 10.14006/j.jzjgxb.2015.10.003.

[10] S. Xu, Hao Wang, and Lei Su, "Degradation law of mechanical properties of Q235 steel plate in neutral salt spray corrosion environment," *Mater. Mech. Eng.*, vol. 40, no. 5, pp. 86–91, 2016.

[11] J. Sheng and J. Xia, "Effect of simulated pitting corrosion on the tensile properties of steel," *Constr Build Mater*, vol. 131, 2017, doi: 10.1016/j.conbuildmat.2016.11.037.

[12] L. Li, M. Mahmoodian, C. Q. Li, and D. Robert, "Effect of corrosion and hydrogen embrittlement on microstructure and mechanical properties of mild steel," *Constr Build Mater*, vol. 170, 2018, doi: 10.1016/j.conbuildmat.2018.03.023.

[13] H. Wang, S. Xu, A. Li, and K. Kang, "Experimental and numerical investigation on seismic performance of corroded welded steel connections," *Eng Struct*, vol. 174, 2018, doi: 10.1016/j.engstruct.2018.07.057.

[14] B. Wang, W. Huang, and S. Zheng, "Study on restoring force performance of corrosion damage steel frame beams under acid atmosphere," *Applied Sciences (Switzerland)*, vol. 9, no. 1, 2019, doi: 10.3390/app9010103.

[15] S. Xu, Z. Zhang, and G. Qin, "Study on the seismic performance of corroded H-shaped steel columns," *Eng Struct*, vol. 191, 2019, doi: 10.1016/j.engstruct.2019.04.037.

[16] C. Jia, Y. Shao, L. Guo, and Y. Liu, "Mechanical properties of corroded high strength low alloy steel plate," *J Constr Steel Res*, vol. 172, 2020, doi: 10.1016/j.jcsr.2020.106160.

[17] K. Woloszyk and Y. Garbatov, "Random field modelling of mechanical behaviour of corroded thin steel plate specimens," *Eng Struct*, vol. 212, 2020, doi: 10.1016/j.engstruct.2020.110544.

[18] X. Zhang, S. Zheng, and X. Zhao, "Experimental and numerical study on seismic performance of corroded steel frames in chloride environment," *J Constr Steel Res*, vol. 171, 2020, doi: 10.1016/j.jcsr.2020.106164.

[19] Y. Wang, T. Shi, H. Zhang, B. Nie, H. Wang, and S. Xu, "Hysteretic behavior and cyclic constitutive model of corroded structural steel under general atmospheric environment," *Constr Build Mater*, vol. 270, 2021, doi: 10.1016/j.conbuildmat.2020.121474.

[20] H. Chen, Z. Chen, T. Zhou, L. Guo, and H. Liu, "Experimental Investigation of Various Corroded Metal Materials Used in Building Structures," *Journal of Materials in Civil Engineering*, vol. 34, no. 12, 2022, doi: 10.1061/(asce)mt.1943-5533.0004498.

[21] Q. Si, Y. Ding, L. Zong, and H. T. Zhao, "MECHANICAL BEHAVIOUR OF CORRODED STRUCTURAL STEEL SUBJECTED TO MONOTONIC TENSION," *Advanced Steel Construction*, vol. 18, no. 3, 2022, doi: 10.18057/IJASC.2022.18.3.8.

[22] L. Jin, X. Zhang, X. Liang, Z. Wang, and Q. Wu, "Mechanical properties of corroded carbon steel based on random pit corrosion in marine environment," *Ocean Engineering*, vol. 260, 2022, doi: 10.1016/j.oceaneng.2022.111759.

[23] Z. Kong *et al.*, “Experimental and theoretical study on mechanical properties of mild steel after corrosion,” *Ocean Engineering*, vol. 246, 2022, doi: 10.1016/j.oceaneng.2022.110652.
[24] T. Zhang, Q. Xu, F. Yang, and S. Gao, “Study on Degradation Law and the Equivalent Thickness Model of Steel Subjected to Sulfate Corrosion,” *Materials*, vol. 16, no. 12, 2023, doi: 10.3390/ma16124320.
[25] X. Zhang, S. Zheng, X. Zhao, and Q. Yang, “Seismic performance and hysteretic model of corroded steel frame columns in offshore atmospheric environment,” *Advances in Structural Engineering*, vol. 26, no. 16, 2023, doi: 10.1177/13694332231208249.
[26] Y. Wang, D. Wang, S. Xu, and C. Guedes Soares, “Experimental study on the low-cycle loading behaviour and constitutive relationships of accelerated corroded steel plates,” *J Constr Steel Res*, vol. 221, p. 108883, 2024, doi: https://doi.org/10.1016/j.jcsr.2024.108883.
[27] S. Chen, W. Zhang, Y. Xu, X. Zhou, Y. Chen, and W. Chen, “Experimental study on the degradation of mechanical properties of H-shaped steel columns in the chloride salt environment,” *J Constr Steel Res*, vol. 217, p. 108670, 2024, doi: https://doi.org/10.1016/j.jcsr.2024.108670.
[28] Z. Kong *et al.*, “Mechanical performance of Q345 steel after corrosion: Experimental and theoretical investigation,” *Structures*, vol. 62, 2024, doi: 10.1016/j.istruc.2024.106264.
[29] L. F. Xiao, J. X. Peng, J. R. Zhang, and C. S. Cai, “Mechanical properties of corroded high performance steel specimens based on 3d scanning,” *Advanced Steel Construction*, vol. 15, no. 2, 2019, doi: 10.18057/IJASC.2019.15.2.2.
[30] L. Xiao, J. Peng, J. Zhang, Y. Ma, and C. S. Cai, “Comparative assessment of mechanical properties of HPS between electrochemical corrosion and spray corrosion,” *Constr Build Mater*, vol. 237, 2020, doi: 10.1016/j.conbuildmat.2019.117735.
[31] J. L. Chaboche, “Constitutive equations for cyclic plasticity and cyclic viscoplasticity,” *Int J Plast*, vol. 5, no. 3, 1989, doi: 10.1016/0749-6419(89)90015-6.
[32] J. Lemaitre and J.-L. Chaboche, *Mechanics of Solid Materials*. 1990. doi: 10.1017/cbo9781139167970.
[33] Voce, “The relationship between stress and strain from homogenous deformation,” *Journal of the Institute for Metals*, vol. 74, 1948.
[34] Dassault Systèmes Simulia, *Abaqus CAE User’s Manual (6.14)*. 2014.
[35] M. DAniello, R. Landolfo, V. Piluso, and G. Rizzano, “Ultimate behavior of steel beams under non-uniform bending,” *J Constr Steel Res*, vol. 78, 2012, doi: 10.1016/j.jcsr.2012.07.003.
[36] AISC, *ANSI/AISC 341-16 Seismic Provisions for Structural Steel Buildings*, no. 2. 2022.
[37] British Standards, *EN 10034: 1993–Structural steel I and H sections—Tolerances on shape and dimensions*. British Standards, 1993.
[38] A. Elkady and D. G. Lignos, “Improved Seismic Design and Nonlinear Modeling Recommendations for Wide-Flange Steel Columns,” *Journal of Structural Engineering*, vol. 144, no. 9, 2018, doi: 10.1061/(asce)st.1943-541x.0002166.
[39] J. L. Chaboche, “Time-independent constitutive theories for cyclic plasticity,” *Int J Plast*, vol. 2, no. 2, 1986, doi: 10.1016/0749-6419(86)90010-0.
[40] Y. Chen, W. Sun, and T. M. Chan, “Cyclic stress-strain behavior of structural steel with yieldstrength up to 460 N/mm2,” *Frontiers of Structural and Civil Engineering*, vol. 8, no. 2, 2014, doi: 10.1007/s11709-014-0245-y.
[41] EN:1998-3:2005-(E), *EN 1998-3. Eurocode 8 - Design of structures for earthquake resistance - Part 3: Assessment and retrofitting of buildings*. 2005.

[42] "Seismic rehabilitation of existing buildings," *ASCE Standard*, no. 41–6, 2007, doi: 10.1201/9781439804810-c7.
[43] R. D. Ziemian, *Guide to Stability Design Criteria for Metal Structures: Sixth Edition*. 2010. doi: 10.1002/9780470549087.
[44] H. El Jisr, A. Elkady, and D. G. Lignos, "Composite steel beam database for seismic design and performance assessment of composite-steel moment-resisting frame systems," *Bulletin of Earthquake Engineering*, vol. 17, no. 6, 2019, doi: 10.1007/s10518-019-00564-w.
[45] M. Araújo, L. Macedo, and J. M. Castro, "Evaluation of the rotation capacity limits of steel members defined in EC8-3," *J Constr Steel Res*, vol. 135, 2017, doi: 10.1016/j.jcsr.2017.04.004.
[46] H. Krawinkler, "Cyclic loading histories for seismic experimentation on structural components," *Earthquake Spectra*, vol. 12, no. 1, 1996, doi: 10.1193/1.1585865.
[47] D. G. Lignos and H. Krawinkler, "Deterioration Modeling of Steel Components in Support of Collapse Prediction of Steel Moment Frames under Earthquake Loading," *Journal of Structural Engineering*, vol. 137, no. 11, 2011, doi: 10.1061/(asce)st.1943-541x.0000376.
[48] A. Standard, *ASCE standard, ASCE/SEI, 41-17, seismic evaluation and retrofit of existing buildings*. 2017.